Eos, Vol. 85, No. 46, 16 November 2004

NASA EOS Sensors Demonstrate Potential for Multiparameter Studies of Arctic Sea Ice

PAGES 481, 488–489

Remote sensing of sea ice is a difficult task due to the discontinuous, complex surface (ice, water, snow) and the frequent presence of clouds. Only through combinations of data from a variety of sensor types can a thorough and complete characterization of sea ice be obtained.

The sensors on the NASA Earth Observing System (EOS) Aqua, Terra, and ICESat satellites represent a substantial step forward in the ability to observe sea ice. The sensors are a significant advancement over their predecessors in terms of spatial and radiometric resolution. The increased variety of geophysical data products from the sensors provides a wealth of new information about sea ice. Combinations of products from the different sensors have the potential to provide additional insights.

Here, this potential of the EOS satellites is demonstrated by presenting an example that uses three sensors on three different EOS satellites to characterize a large lead (an opening in the sea ice resulting from ice dynamics) in the Beaufort Sea during March 2004.

The sensors include the Advanced Microwave Scanning Radiometer for EOS (AMSR-E) on the Aqua spacecraft; the Moderate Resolution Imaging Spectroradiometer (MODIS) on board both the Aqua and Terra spacecraft; and the Geoscience Laser Altimeter System (GLAS) on the Ice, Cloud, and land Elevation Satellite (ICESat). AMSR-E and MODIS provide improved passive microwave and visible/infrared products, respectively, and GLAS is the first satellite-borne Earth-observing laser altimeter, representing an entirely new technology for sea ice remote sensing.

The sea ice (and other) geophysical products and documentation for the EOS sensors are archived at the National Snow and Ice Data Center (NSIDC) Distributed Active Archive Center (DAAC) in Boulder, Colorado. Data products and documentation can be accessed from NSIDC at http://nsidc.org/daac/projects.html. The authors include the NSIDC product team leads of AMSR-E, MODIS, and ICESat who work closely with the respective sensor science teams.

Along with improved products, the new generation of sensors also provides standardized, self-descriptive data access through the standard Hierarchical Data Format (HDF) or HDF-Earth Observing System (HDF-EOS) formats, which are accessible through a variety of standard image and data processing software. Additional tools are also available from NSIDC at http://nsidc.org/data/tools/.

By W. N. Meier, M. Marquis, M. Kaminski, and R. Weaver

Background on Sensors

AMSR-E's six dual-polarized passive microwave frequencies represent the next step in passive microwave remote sensing and are a substantial improvement over predecessor sensors, including the Special Sensor Microwave/Imager (SSM/I) and the Scanning Multichannel Microwave Radiometer (SMMR). AMSR-E's higher spatial resolution and additional frequencies compared with SSM/I (Table 1) have the ability to provide improved products, as well as entirely new products.

AMSR-E provides continuity with the 25+ year historical record of sea ice concentrations, but at double the spatial resolution (Table 1) and with improved algorithms. For AMSR-E, the Enhanced NASA Team Sea Ice Algorithm (also called NASA Team 2) is used for the Arctic and a modified Bootstrap Sea Ice Algorithm is used for the Antarctic.

These ice concentration products are still being validated through various studies, including Antarctic field projects in 2003 and 2004 (T. Markus and J. Comiso, personal communication, 2004) and Arctic field projects (D. Cavalieri, personal communication, 2004); further information on AMSR-E validation studies is available at http://nsidc.org/data/amsr_validation/cryosphere/. The sea ice concentration algorithms incorporate several refinements over the standard algorithms for SSM/I, and initial indications are that AMSR-E represents a substantial improvement over SSM/I [*Comiso et al.*, 2003].

Other standard AMSR-E products include sea ice temperature and snow depth over sea ice (only first-year ice in the Arctic), which are not available from previous satellite passive microwave sensors (Table 1). (The sea ice temperature is indicative of the temperature of the emitting layer, which often corresponds to the sea ice/snow interface.) Validation of these new sea ice products is also ongoing. All AMSR-E sea ice fields are produced on a polar stereographic grid as daily composites of ascending, descending, and all passes over a 24-hour period; swath brightness temperatures are also available.

More information on the sea ice products is available in *Comiso et al.* [2003] and on the NSIDC Web pages. Updated products containing further refinements in the algorithms based on the validation studies are scheduled to be released in the coming year.

MODIS observes the Earth at 36 visible and infrared spectral bands ranging from 0.405–14.385 μm at a spatial resolution ranging from 250 to 1000 m. MODIS represents a substantial improvement in spectral range and spatial resolution over its predecessor, the Advanced Very High Resolution Radiometer (AVHRR), which contains only five spectral bands (0.63–12 μm) and a resolution of 1 or 4 km. Thus, MODIS yields much improved information on sea ice properties over AVHRR.

MODIS provides several sea ice products, including sea ice extent and surface temperature (Table 1). More information and an initial evaluation of the sea ice surface temperature product used in the example below are available in *Hall et al.* [2004]; further validation of the MODIS sea ice products is ongoing.

ICESat/GLAS is the first satellite Earth-observing laser altimeter, and it produces a unique suite of remotely sensed sea ice products. The laser altimeter measures the topography of features on Earth's surface at two frequencies, one green (532 nm) and one infrared (1064 nm). The most relevant ICESat/GLAS parameters for sea ice are its elevation and roughness.

The active laser on ICESat/GLAS also has particular advantages over passive visible and infrared sensors in detecting clouds and cloud properties. This is especially beneficial over ice-covered surfaces where the surface and clouds can be difficult to distinguish from each other when using passive visible and infrared sensors.

Due to postlaunch sensor problems, data over only limited time periods will be available from ICESat. Releases of improved products are ongoing as algorithm refinements are made. Validation of the ICESat sea ice products has been limited, but initial results indicate root mean square (RMS) accuracies over sea ice of 5–10 cm [*Zwally et al.*, 2003]. A preliminary study indicates that ICESat/GLAS, when combined with other sensors such as Radarsat, is potentially even more accurate (~2 cm RMS), and can provide useful and unique estimates of sea ice thickness and total ice mass [*Kwok et al.*, 2004].

Combination of Sensor Products to Study an Arctic Lead

Combining multiple products from multiple sensors yields more complete information about sea ice processes. To illustrate the potential of the new EOS products, a case study is presented in the Beaufort Sea during early March 2004 (Figure 1, left).

As seen in daily composite 89-GHz imagery (Figure 1, middle), in the Beaufort Sea north of Barrow, Alaska, a thinner lead (A), open on 2 March, closes between 2 and 3 March, and is replaced by a much wider lead (B) to the east. A coastal polynya (C), a semi-permanent open-water region within the sea ice created by winds or ocean upwelling, also forms to the west of Barrow. Lead B is upward of 25 km wide in some areas, and several hundred kilometers long. No single sensor or product can retrieve all information of interest about the environment in and around the lead. However, through the combination of products from the three sensors, the lead opening and

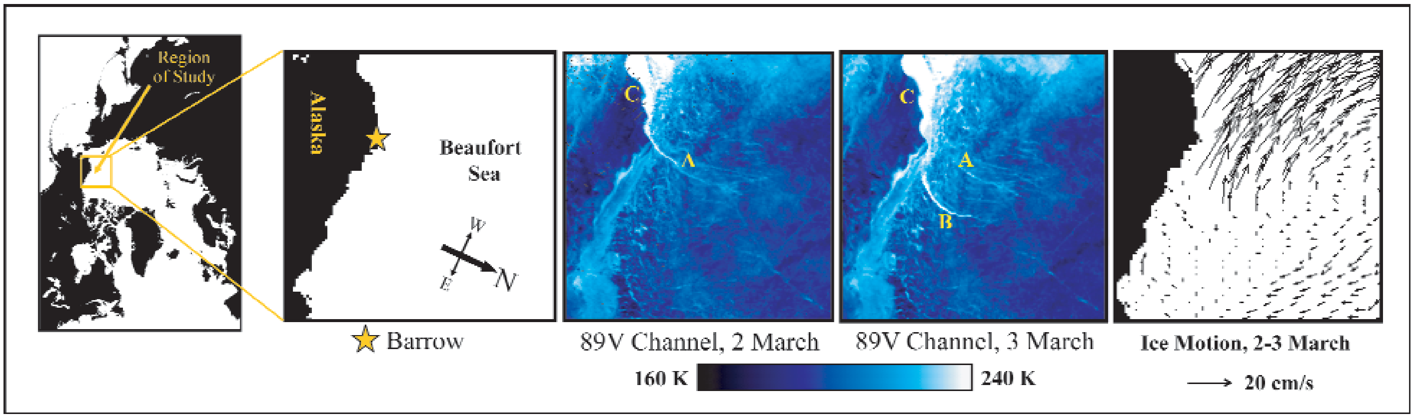

Fig. 1. (left to right) Map of Arctic region; blowup of region of interest in the Beaufort Sea; vertically polarized 89-GHz AMSR-E brightness temperature (T_B) for 2 March 2004; 89V T_B for 3 March 2004; and 24-hour sea ice motion derived from the 2 and 3 March 89V T_Bs. The three sea ice openings of note in the 89-GHz imagery are the initial lead (A), the larger lead (B) that forms between 2 and 3 March, and the coastal polynya (C). The appearance of lead B in the 89V image of 3 March is the result of the strong divergence off the coast of Barrow apparent in the motion field.

refreezing process can be more completely investigated.

An experimental product of daily sea ice motions derived from daily 89-GHz vertically polarized Tb fields shows strong divergent motion (Figure 1, right) west of Barrow on 2–3 March, causing the large lead (B) to form. There is also a strong offshore flow west of Barrow, resulting in the coastal polynya (C). Circulation changes on 4–5 March (not shown) turn the flow onshore and lead B starts closing. The motions are estimated using a maximum cross-correlation scheme that matches features in co-located image pairs [*Emery et al.*, 1991].

The AMSR-E 19-GHz and 37-GHz channels used for sea ice concentration have a larger footprint and thus cannot resolve lead B in detail; even at its widest on 4 March, the lead is seen in the concentration field only as a small region of reduced ice concentration (Figure 2, left). AMSR-E does, however, resolve the coastal polynya near Barrow. The following day, under clear skies on 5 March, the higher spatial resolution (500 m) of MODIS clearly indicates warmer temperatures in the lead and resolves many other fracture features west (above the lead in the image) of the lead (Figure 2, right); the cooler (below freezing) surface temperatures on the leeward side of the lead show where freezing has begun. Clouds contaminate temperatures east of the lead. The coastal polynya near Barrow is also clearly visible.

In an overpass of the lead on 7 March, ICESat/GLAS also detects the lead, clearly visible as a thinner, smoother region of the transect (Figure 3). The freeboard/draft was estimated from the standard GLAS sea ice elevation product, with corrections made for the geoid and the dynamic topography; this correction simply calibrates sea level to the lowest elevation in the vicinity and ignores clouds and other possible error sources. However, it does appear to yield a fair representation of the ice cover, particularly the lead.

By 7 March, the ICESat/GLAS data indicate that the lead is completely frozen over (i.e., the ice thickness is greater than zero across the entire lead). Using nearby Barrow air temperatures from the National Oceanic and Atmospheric Administration and Lebedev's ice growth equation (based on freezing degree days) yields a theoretical thickness of 0.16 m for the thinnest ice in the lead, which is quite close to the estimate from the ICESat/GLAS transect (Figure 3, right). The transect also shows thicker ice on the leeward side of the lead where ice growth began earlier and where rafting/ridging may be occurring.

ICESat/GLAS also produces fields of atmospheric parameters such as cloud and aerosol properties, although these products were not investigated in this study; such products are

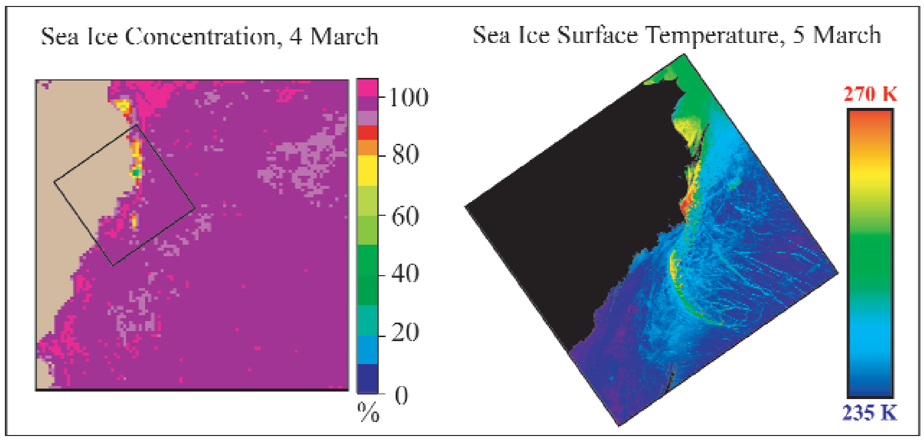

Fig. 2. (left) AMSR-E sea ice concentration, with the colors indicating percent of areal coverage in a 12.5-km pixel. (right) MODIS ice surface temperature in a subregion of the sea ice concentration image (outlined in the black box) containing the lead.

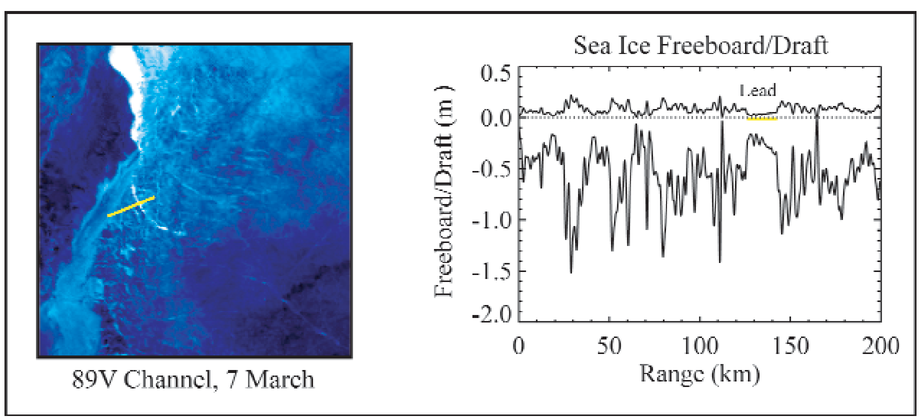

Fig. 3. (left) AMSR-E 89V Tb for 7 March with the section of the ICESat transect overlaid in yellow. (right) Sea ice freeboard and draft derived from elevation data from ICESat/GLAS on 7 March; the area of the lead is clearly visible in the transect as thinner and smoother ice (highlighted in yellow).

Table 1. Sensor Properties and Sea Ice Products for MODIS and AMSR-E.

AMSR-E and SSM/I Sensor Properties					
Frequency (GHz)		IFOV (km)		Maximum Gridded Resolution (km)	
SSM/I	AMSR-E	SSM/I	AMSR-E	SSM/I	AMSR-E
-	6.9	-	75 x 43	-	25
-	10.7	-	51 x 29	-	25
19.3	18.7	70 x 45	27 x 16	25	12.5
22.2	23.8	60 x 40	31 x 18	25	12.5
37.0	36.5	38 x 30	14 x 8	25	12.5
85.5	89.0	16 x 14	6 x 4	12.5	6.25

AMSR-E and SSM/I Sea Ice Products		
Sea Ice Product	Gridded Resolution (km)	
	SSM/I	AMSR-E
19, 37 GHz T_B	25	12.5, 25
85.5/89 GHz T_B	12.5	6.25, 12.5, 25
Concentration	25	12.5, 25
Snow Depth*	-	12.5
Temperature	-	25

MODIS Sea Ice Products	
Product	Resolution (km)
Swath Sea Ice Extent	1.0
Daily Global Sea Ice Extent (Day and Night Fields)	1.0, 4.0
Daily Global Sea Ice Surface Temperature (Day and Night Fields)	4.0

*SSM/I properties are provided with AMSR-E for comparison. IFOV = instantaneous field-of-view (i.e., footprint). *AMSR-E snow depth calculated over first-year sea ice only.*

potentially valuable for estimating air-sea fluxes over the lead.

Other new insights into the character of sea ice from the combination of the EOS sensors, as well as through combinations with other non-EOS sensors, will likely be developed in the coming years. As previously mentioned, a combination of ICESat/GLAS data with Radarsat imagery has already been used to estimate lead openings in the sea ice [*Kwok et al.*, 2004].

The combination of passive microwave imagery, visible/infrared imagery, and laser altimetry provides a more complete characterization of the sea ice environment than was previously possible. Frequent, high-resolution products provide accurate estimates of important sea ice parameters such as ice concentration, ice temperature, ice thickness, and snow cover. These will provide valuable insights into the changing Arctic environment, and the improved data will be beneficial as model inputs to produce improved forecasts of future climate change.

Acknowledgments

Thanks to NASA (contract NAS5-03099) for support of archival of EOS data at NSIDC. ICESat/GLAS data courtesy of B. Schutz, H. J. Zwally, and the ICESat/GLAS science team. Assistance with ICESat/GLAS data provided by M. Savoie, T. Haran, and T. Scambos of NSIDC. MODIS image provided by J. Wolfe of NSIDC.

References

Comiso, J. C, D. J. Cavalieri, and T. Markus (2003), Sea ice concentration, ice temperature, and snow depth using AMSR-E data, *IEEE Trans. Geosci. Remote. Sens.*, *41(2)*, 243–252.

Emery, W. J., C. W. Fowler, J. Hawkins, and R. H. Preller (1991), Fram Strait satellite image-derived ice motions, *J. Geophys. Res.*, *96(C5)*, 8917–8920.

Hall, D. K., J. R. Key, K. A. Casey, G. A. Riggs, and D. J. Cavalieri (2004), Sea ice surface temperature product from MODIS, *IEEE Trans. Geosci. Remote. Sens.*, *42(5)*, 1076–1087.

Kwok, R., H. J. Zwally, and D. Yi (2004), ICESat observations of Arctic sea ice: A first look, *Geophys. Res. Lett.*, *31*, L16401, doi:10.1029/2004GL020309.

Zwally, H. J., A. C. Brenner, S. L. Farrell, S. W. Laxon, and D. Yi (2003), Deriving sea-ice freeboard height distributions and estimates of ice thickness from ICESat/GLAS laser altimetry, *Eos Trans. AGU*, *84*(46), Fall Meet. Suppl., Abstract C32A-0442.

Author Information

Walter N. Meier, Melinda Marquis, Marilyn Kaminski, and Ron Weaver, National Snow and Ice Data Center, University of Colorado, Boulder

For additional information, contact W. N. Meier; E-mail: walt@nsidc.org.

Ancient Oak Climate Proxies From the Agricultural Heartland

PAGE 483

Understanding the long-term variability in climate has important societal implications, particularly for agricultural regions that are suppliers to global food markets such as the central United States. Paleoclimate information from agriculturally important regions of the central United States is limited in length and resolution.

Tree rings provide one of the longest and highest-resolution paleoclimate records for North America; however, millennium-length records are primarily from extreme environments (e.g., deserts, cliffs, high elevations) and do not represent climate-plant responses in the central U.S. agricultural region.

By R. P. Guyette, M. C. Stambaugh, and D. C. Dey

Recent research on the abundance and dendrochronology (tree-ring record) of modern and subfossil oak (*Quercus macrocarpa*, *Quercus bicolor*) collected from streams in Missouri and Iowa (93°18'W, 40°22'N) may enable the development of one of the longest tree-ring records in the world, with initial data suggesting that the construction of a Holocene-length-plus proxy climate record is possible. The importance of constructing this record lies in its ability to provide information concerning past climate variability and timing of specific climatic events.

This article reports on the American Long Oak Chronology (ALOC), a new research effort that aims to understand the past environmental conditions of the U.S. agricultural heartland from the construction of a Holocene-length tree-ring record.

Previous contributions of millennium-length tree-ring chronologies to geoscience have been extraordinary. One of the most notable contributions of these data has been the development and use of high-precision radiocarbon calibration curves.

In addition, tree-ring chronologies have provided a significant proportion of paleoecological information that includes air temperature, hydroclimate, fire, frost, and streamflow reconstructions, various scales of spatial and temporal variability in atmospheric circulation, climate change model calibration, and estimates of long-term agricultural productivity. This list outlines only some of the potential uses of the ALOC. Additional uses might include studies of volcanology, glaciology, and carbon budgets [*Guyette et al.*, 2002].

The ALOC Resource

Previously, long tree-ring chronologies developed from subfossil oak wood have been limited to areas in the British Isles and Germany